MODELLING THE RADIOLYTIC CORROSION OF NUCLEAR FUEL INSIDE A FAILED WASTE CONTAINER

N. Liu[1], L. Wu[2], Z. Qin[1] and D.W. Shoesmith[1]
[1] Western University, London, Ontario, Canada
[2] Canadian Nuclear Laboratories, Chalk River, Ontario, Canada
dwshoesm@uwo.ca, nliu63@uwo.ca, linda.wu@cnl.ca, zqin@uwo.ca,

Abstract

The international concept for the disposal of high level nuclear waste involves multiple barriers including the fuel bundles, durable metal containers, clay buffer and seals, and a deep geologic environment. A key barrier in the Canadian concept is the corrosion resistant container which consists of an outer copper barrier and an inner carbon steel vessel. While designed not to fail, it is judicious to examine the consequences of container failure when the used fuel bundles could be exposed to groundwater leading to their radiolytic corrosion and the release of radionuclides to the groundwater.

If failure occurs two corrosion fronts will be established; one on the fuel driven by the alpha radiolysis of water and a second one on the inside of the steel vessel leading to the dissolution of Fe^{2+} and the production of H_2.

Both 1-dimensional and 2-dimensional models have been developed to determine the influence of redox conditions within the failed container on the fuel corrosion/radionuclide release process. These models take into account water radiolysis, the reaction of radiolytic H_2O_2 with the fuel both directly and via galvanic coupling to fission product phases in the fuel, the reaction with H_2 (from steel corrosion and water radiolysis) catalyzed on the fuel surface and the scavenging of radiolytic H_2O_2 by reaction with Fe^{2+}.

The models are described by 1-dimensional diffusion reaction equations and solved numerically using COMSOL Multiphysics, a commercial simulation package based on the finite element model. The 1-dimensional model attempts to calculate corrosion rates on the exposed surface of fuel pellets while the 2-dimensional model attempts to determine the corrosion behaviour within the cracks in the fuel pellet. Despite extensive international efforts the available database is limited. The sensitivity to various reactions in the model will be evaluated and the necessary improvements identified.

1. Introduction

The recommended approach for the long-term management of used nuclear fuel in Canada is adaptive phased management [1]. As accepted internationally, the repository concept is based on multiple barriers including the fuel bundles, durable metal containers with an outer layer of copper and an inner carbon steel vessel, a clay buffer and seals around the container, and a deep geologic environment [2]. A key

barrier in this sequence is the corrosion-resistant container that is expected to isolate the used fuel from the repository environment [3, 4]. However, it is judicious to examine the consequences of container failure and the exposure of used fuel bundles to groundwater.

In the anoxic conditions anticipated in a deep geological repository, water radiolysis, resulting from the radiation fields associated with the used fuel, will be the only source of oxidants within a failed groundwater-containing container. The key radiolysis product, H_2O_2, has been shown to be the primary oxidant driving fuel corrosion [5]. Oxidation of fuel (U^{IV}) will produce the oxidized form (U^{VI}) with a considerably higher solubility than U^{IV}, leading to the release of radionuclides [6]. Another corrosion front, sustained by water reduction to produce the potential redox scavengers, Fe^{2+} and H_2, is present on the inner surface of the carbon steel vessel.

The development of radiolytic models (in particular for α-radiolysis) for spent fuel corrosion has recently been reviewed [7]. A mixed potential model based on electrochemical parameters for fuel corrosion was developed [8]. Jonsson et al. developed a comprehensive model which integrated the available kinetic data and tried to account for the geometrical distribution of the radiation dose rate at the surface of the fuel and the effects of the oxidant scavengers Fe^{2+} and H_2, fuel burn up, and ground water chemistry [9]. In this paper, we will review our work of the development of the 2-dimensional models of radiolytic corrosion of spent nuclear fuel inside a failed waste container.

2. Chemical reactions included in the model

Under irradiation the fuel undergoes a number of microstructural and compositional changes involving the formation of rare earth (RE^{III}) elements and noble metal (ε) particles, which have been shown to influence its chemical reactivity under anticipated disposal conditions [10]. The RE^{III} elements cause an increase in the electrical conductivity of the fuel matrix and the noble metal particles, generally segregated to grain boundaries, can act as either cathodes or anodes (depending on the prevailing redox conditions in the exposure environment) galvanically-coupled to the conductive RE^{III}-doped UO_2 matrix.

Figure 1 illustrates the two corrosion fronts within the container and the main reactions involved in controlling redox conditions and, hence, the process of fuel corrosion. The model includes: (1) the production of H_2O_2 and H_2 by water radiolysis; (2) the oxidative dissolution (corrosion) of UO_2 supported by H_2O_2 reduction on both the UO_2 surface (reaction 2a) and noble metal particles (reaction 2b); (3) the reduction of oxidized surface species (U^V/U^{VI}) by H_2 oxidation on noble metal particles (reaction 3a) and of dissolved UO_2^{2+} either by reaction with H_2 in solution (reaction 3b) or with H_2 catalyzed on the fuel surface (reaction 3c); (4) the scavenging of H_2O_2 in homogeneous solution by reaction with Fe^{2+}; (5) the reaction of H_2O_2 with H_2 catalyzed by noble metal particles; and (6) the decomposition of H_2O_2 to O_2 and H_2O. Some of the reactions will be discussed in detail.
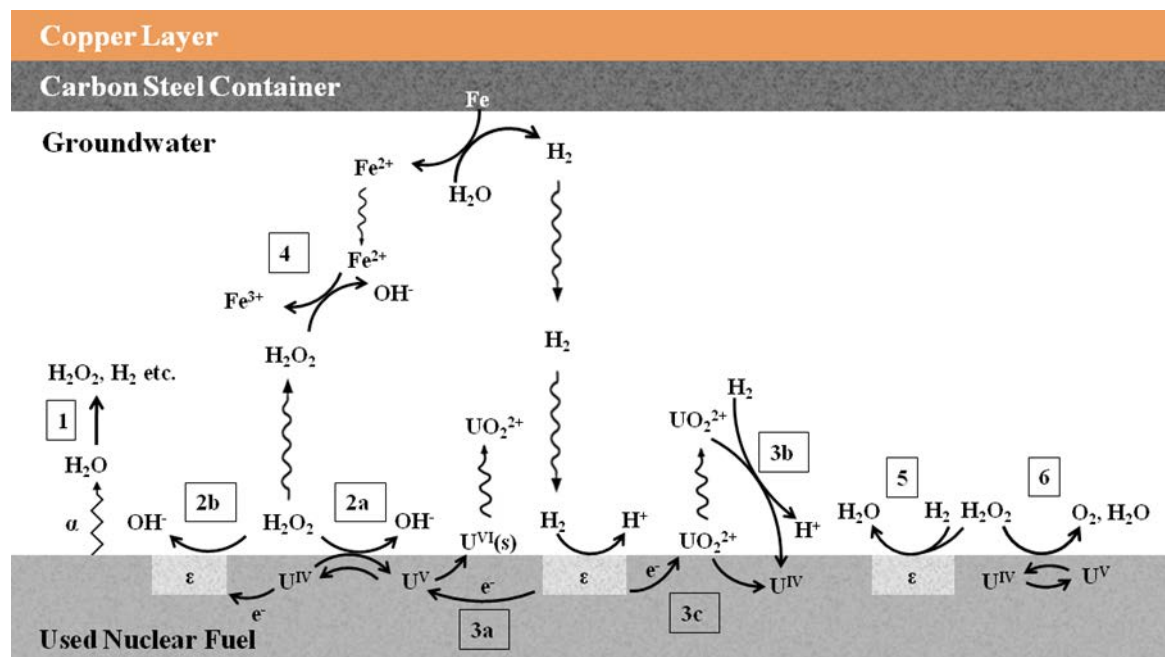
Figure 1. Schematic illustration of the reactions included in the model for the
α-radiolytic corrosion of spent nuclear fuel [11].

2.1 Water radiolysis

It is reasonable to assume that waste containers will remain unbreached over the period when β/γ radiation fields are significant, thus, only α-radiolysis is considered as a source of oxidants in a failed container. In the original 1-dimensional model [12], only H_2O_2 is considered as the product of water radiolysis. However, the interaction of α-radiation with water yields a series of decomposition products (H_2, H_2O_2, H•, OH•, HO_2•,e_{aq}^-, H^+ and OH^-), so in the improved 1-dimensional model [11], a full radiolytic reaction set was incorporated. The analysis result shows that a simplified calculation which only accounts for the radiolytic production of molecular products (H_2O_2/H_2) would provide a reasonable and conservative approximation.

In the present model, water radiolysis can happen in a very thin layer of water (13 μm) above the fuel surface where the dose rate is uniformly distributed [13]. This simplification was justified by comparing the UO_2^{2+} flux based on either the uniform or exponential dose distribution. The sensitivity test shows that the former is a conservative approach.

2.2 U^V/U^{VI} reduction by H_2

Hydrogen has been shown to suppress UO_2 corrosion on a range of UO_2 materials ranging from spent fuel itself to α-doped UO_2 and SIMFUELs. There appear to be three possible pathways for reaction between U^V/U^{VI} and H_2 as numbered in Fig. 1. Reaction 3c (Figure 1), the reduction of adsorbed UO_2^{2+} by H_2 catalyzed on the surface of noble metal particles, has been studied by Nilsson et al [14]. Based on experiments using Pd (to simulate noble metal particles) in an aqueous UO_2^{2+}

solution with a H_2 atmosphere, it is claimed that the reaction rate is independent of the dissolved $[H_2]$ when varying the H_2 pressure between 1.5 and 40 bar, and can be represented by the rate equation (1) in which s_ε is the fractional surface coverage by ε-particles (taken to 0.01), and k_{3c} is the rate constant measured to be 1.5×10^{-5} m s^{-1}[14].

$$R_{3c} = k_{3c} [UO_2^{2+}] s_\varepsilon \qquad\qquad (1)$$

The lowest $[H_2]$ used in this study was 1.17×10^{-3} M (the solubility at a pressure of 1.5 bar). However, fuel corrosion kinetics are expected to be influenced by $[H_2]$ at much lower $[H_2]$, and a reasonable assumption is that the reaction kinetics would eventually become first order with respect to both H_2 and UO_2^{2+}, as indicated in rate equation (2),

$$R_{3c} = k'_{3c} [UO_2^{2+}] [H_2] s_\varepsilon \qquad\qquad (2)$$

In order to use rate equation 2 it is necessary to specify a value for the rate constant which has not been measured. Three possible scenarios are plotted in different colors in Figure 2 showing how the kinetics of reaction 3c could change as the $[H_2]$ is approaching zero: (1) (red), the reaction could become first order to H_2 immediately after the $[H_2]$ falls below the minimum concentration (1.17×10^{-3} M) in the published measurements; (2) (green), the reaction could remain independent of $[H_2]$ to lower concentrations before becoming first order; and (3) (blue), the rate could change non-linearly with $[H_2]$. In the model presented here, the first scenario (red) is adopted with the slope of the red line yielding a rate constant of $k'_{3c} = 1.3 \times 10^{-5}$ [m^4 s^{-1} mol^{-1}]. This scenario is conservative from the perspective of fuel corrosion since the other two scenarios would yield larger rate constants which would lead to faster reduction of UO_2^{2+}.

A similar approach has been adopted in selecting the rate constant for the reduction of H_2O_2 by H_2 catalyzed on noble metal particles (reaction 5 in Figure 1), the rate of which has been shown to be independent of $[H_2]$ over the pressure range 1 to 40 bar [15]. This leads to a modified reaction rate constant, $k'_5 = 2.8 \times 10^{-5}$ [m^4 s^{-1}mol^{-1}].
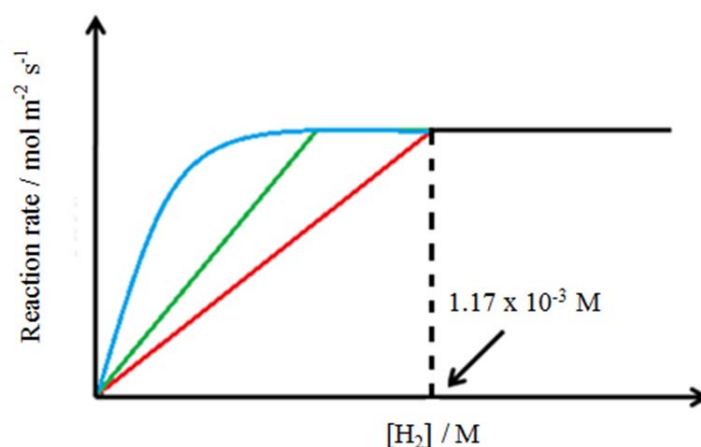
Figure 2. Three possible scenarios for the transition in reaction kinetics for reaction 3c (Figure 1) when [H_2] approaches zero. The dashed line shows the lower bound of experimental measurements (1.17 x 10^{-3} M) above which the reaction rate is independent of [H_2].

2.3 H_2O_2 decomposition

The sensitivity test shows the corrosion rate of UO_2 is very sensitive to H_2O_2 decomposition. The H_2O_2 decomposition rate is sensitive to many features including temperature, pH and the presence of solid/soluble catalysts. The uncertainty about disposal conditions makes the choice of a rate constant arbitrary. Nilsson et al. [16] and Pehrman et al. [17] studied the kinetics of the catalytic decomposition of H_2O_2 on different UO_2 pellets (pure UO_2, doped UO_2, and SIMFUEL) by monitoring the OH· production and concluded that the decomposition rate was virtually independent of matrix doping. They also measured the dissolution yield based on the ratio between the concentrations of dissolved U^{VI} and consumed H_2O_2 and attributed the difference between them to the catalytic decomposition of H_2O_2. These results indicate that the surface-catalyzed decomposition of H_2O_2 is the major pathway for its consumption as opposed to H_2O_2-promoted UO_2 dissolution. Interestingly, the dissolution yield for the pure UO_2 pellet (14%) was much higher than that for the SIMFUEL pellet (0.2%). In the model, 14% of H_2O_2 consumption on the UO_2 surface (not including ε-particles) went to fuel dissolution and the remainder, 86%, to H_2O_2 decomposition.

3. The fracture geometry in the 2-dimensional model

Figure 3 shows a cross section of the fuel/solution interface illustrating the simplified geometry adopted to simulate radiolytic corrosion inside a fracture in a fuel pellet. Radiolysis is considered to occur uniformly within a thin layer of solution on the fuel surface with a thickness of 13 μm [13], given by the average penetration distance of α-radiation in water. Beyond this layer no radiolysis products are produced. The boundary of the uniform radiation zone on the fuel surface is indicated by dashed lines in Figure 2. The diffusion zone is the H_2O layer on the fuel surface over which species can diffuse, and beyond which uniform concentrations are presumed to prevail. The consequences of varying this distance have been shown to be minor [12]. The [H_2] and [Fe^{2+}] are uniform in the bulk solution (i.e., beyond the diffusion zone) and are assumed to depend on the corrosion behaviour of the steel vessel. The concentrations of all radiolytic species and fuel corrosion products are assumed to be zero in the bulk solution beyond the diffusion zone. The average alpha dose rate used in all calculations is 9.03 x 10^5 Gy.a^{-1} corresponding to CANDU fuel with a burnup of 220 MWh.kgU^{-1} at 1000 years after discharge from reactor [13].

The mathematical model is numerically solved using COMSOL Multiphysics based on the finite element method. The model was simulated using the chemical engineering and the dilute species transportation modules (version 4.3.0.151, COMSOL Inc.).
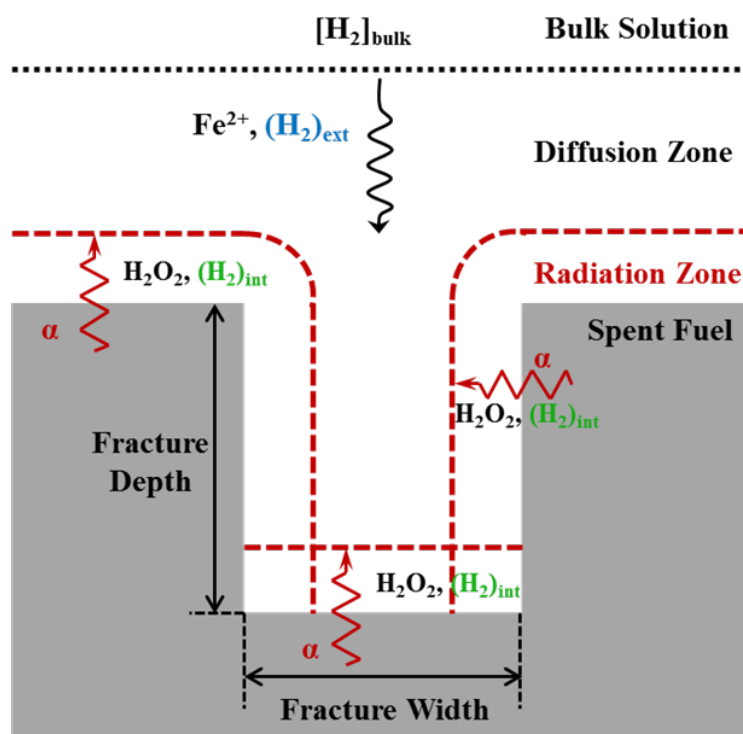
Figure 3. Model arrangement showing a cross section of the fuel/solution interface for the simulation of radiolytic corrosion inside a fracture in a fuel pellet.

4. The influence of fracture geometry on the critical [H$_2$] ([H$_2$]$_{crit}$)

The critical [H$_2$] ([H$_2$]$_{crit}$) is defined as the minimum [H$_2$]$_{bulk}$ required to completely suppress fuel corrosion when the [UO$_2^{2+}$] becomes zero. Figure 4 shows the [H$_2$]$_{crit}$ calculated for a range of fracture dimensions using the adopted rate constants. For wide fractures (i.e., with a width > 0.6 mm), [H$_2$]$_{crit}$ increases as the fracture depth increases. However, for narrow fractures (width < 0.6mm) [H$_2$]$_{crit}$ first increases then decreases as the fracture deepens, suggesting a significant suppression of fuel corrosion by the local accumulation of radiolytically-produced H$_2$, (H$_2$)$_{int}$. Figure 4 also suggests the existence of an upper limit (5.7 µmol L^{-1}, as indicated by the horizontal dashed line) for the [H$_2$]$_{crit}$ for the anticipated range of possible fracture geometries. This value is ~30 times the [H$_2$]$_{crit}$ required on the planar unfractured surface (~0.19 µmol L^{-1}) [11]. This upper limiting value suggests that, if the corrosion of the carbon steel canister can produce a [H$_2$]$_{bulk}$ > 5.7µmol L^{-1}, the corrosion of CANDU spent fuel with the reference burn-up level of 220 MWh.kgU^{-1} should be completely suppressed.
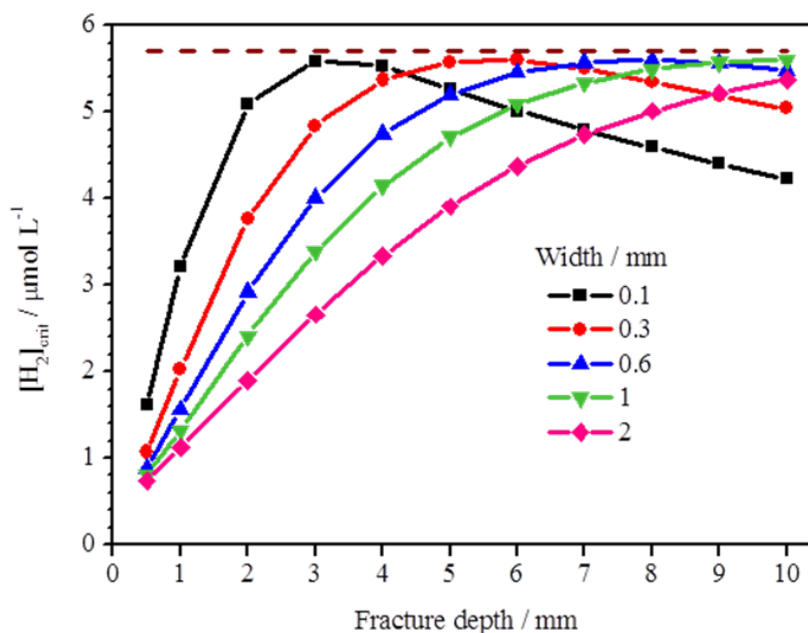
Figure 4. The critical $[H_2]$ ($[H_2]_{crit}$) in fractures with different widths and depths for CANDU spent fuel with a burnup of 220MWh kg U^{-1} at 1000 years after discharge from reactor. The dashed line indicates an upper limit, 5.7 μmol L^{-1}, for the $[H_2]_{crit}$. All other model parameters have the default values.

5. The separation of the effects of internal and external H_2 on the corrosion of a fracture wall

The plots in Figure 4 indicate a significant role for $[H_2]_{int}$ in the suppression of corrosion in narrow and deep fracture locations. This offers the prospect that the demand for $(H_2)_{ext}$ will be considerably lower than expected and the limitations on its transport to these deep locations will not prevent the suppression of fuel corrosion. The separation of the influences of $(H_2)_{int}$ and $(H_2)_{ext}$ is experimentally extremely difficult but can be investigated via modelling. Because the separate H_2 effects on the corrosion rate should be proportional to their respective concentrations, the ratio of $[H_2]_{int}$ to the $[H_2]_{total}$ (total of $(H_2)_{int}$ + $(H_2)_{ext}$) along the wall of the fracture defines the fractional influence of $(H_2)_{int}$. Similarly, the ratio $[H_2]_{ext}/[H_2]_{total}$ along the wall of the fracture defines the fractional influence of $(H_2)_{ext}$.

Figure 5 shows the concentration profiles for $(H_2)_{int}$ for fractures with different depths (0.5, 1, 3 and 6 mm) and a constant width (0.6 mm). As the fracture becomes deeper, $(H_2)_{int}$ accumulates at the bottom of the fracture as its loss by diffusion out of the fracture becomes limited.
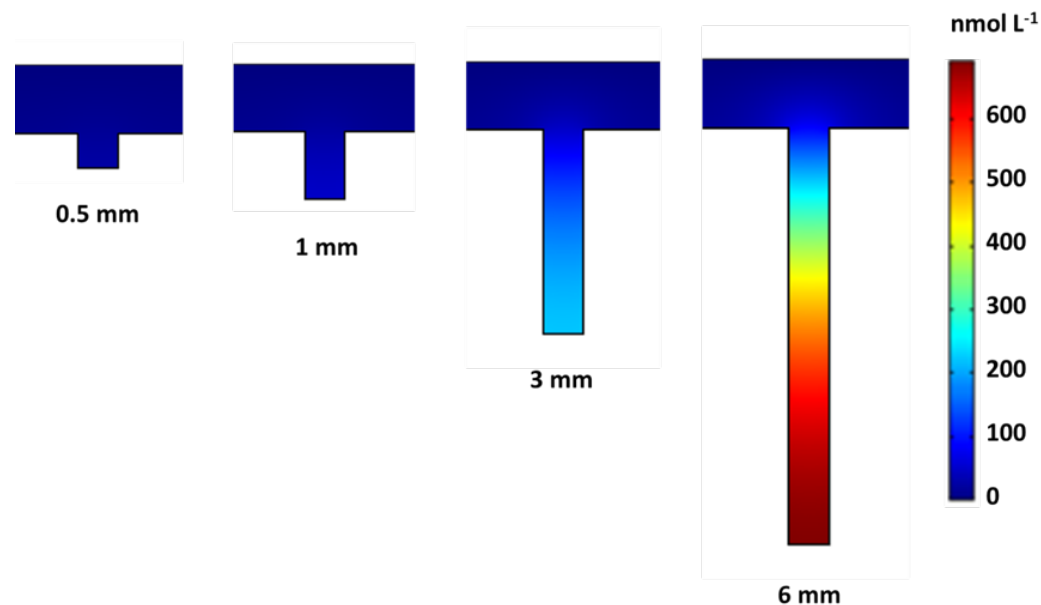
Figure 5. Concentration profiles for $(H_2)_{int}$ in fractures with different depths (0.5, 1, 3 and 6 mm) and a constant width (0.6 mm); $[H_2]_{bulk} = 10^{-8}$ M; all other model parameters have the default values. A schematic description of the fracture is shown in Figure 2.

Figure 6 shows the fractions of $(H_2)_{int}$ and $(H_2)_{ext}$ used in suppressing corrosion as a function of the normalized distance from the base of fractures of various depths. In this case, the bulk $[H_2]$ (supplied by steel canister corrosion) is low (10^{-8} M) and the fuel has a relatively high dose rate (9.03×10^5 Gy a^{-1}) (producing radiolytic H_2). Thus, for the geometries tested, the radiolytic H_2 $((H_2)_{int})$ is always more important than H_2 from steel corrosion $((H_2)_{ext})$. As the fracture becomes deeper the influence of $(H_2)_{int}$ in suppressing corrosion of the walls of the fracture becomes dominant increasing from ~ 70% (0.5 mm depth) to ~98% (6 mm depth).
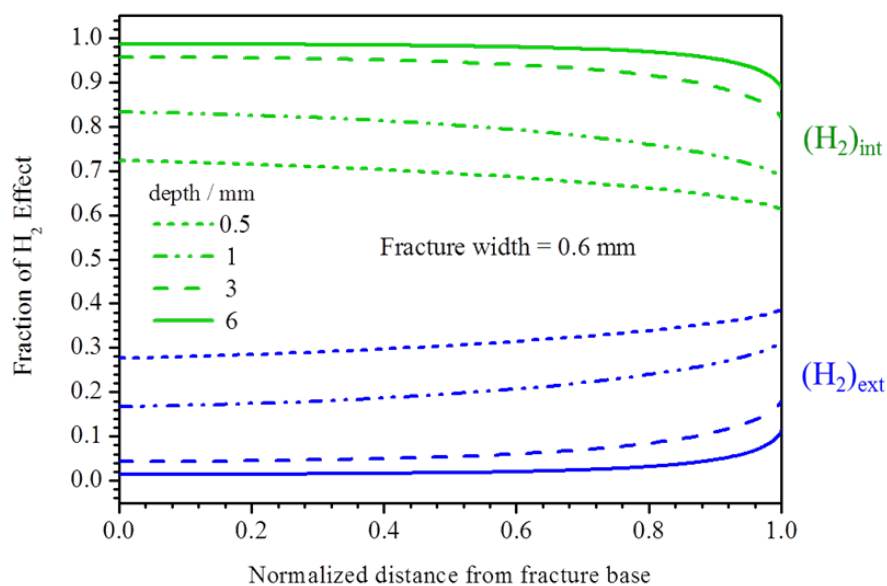
Figure 6. The fractional influences of $(H_2)_{int}$ (green) and $(H_2)_{ext}$ (blue) for different fracture depths (0.5, 1, 3, and 6 mm) with a constant fracture width (0.6 mm); $[H_2]_{bulk} = 10^{-8}$ M; all other model parameters have the default values.

Figure 7 shows that as the fracture gets narrower, there is a greater accumulation of the $(H_2)_{int}$ within the fracture, resulting in an increasing fraction of the $(H_2)_{int}$ effect
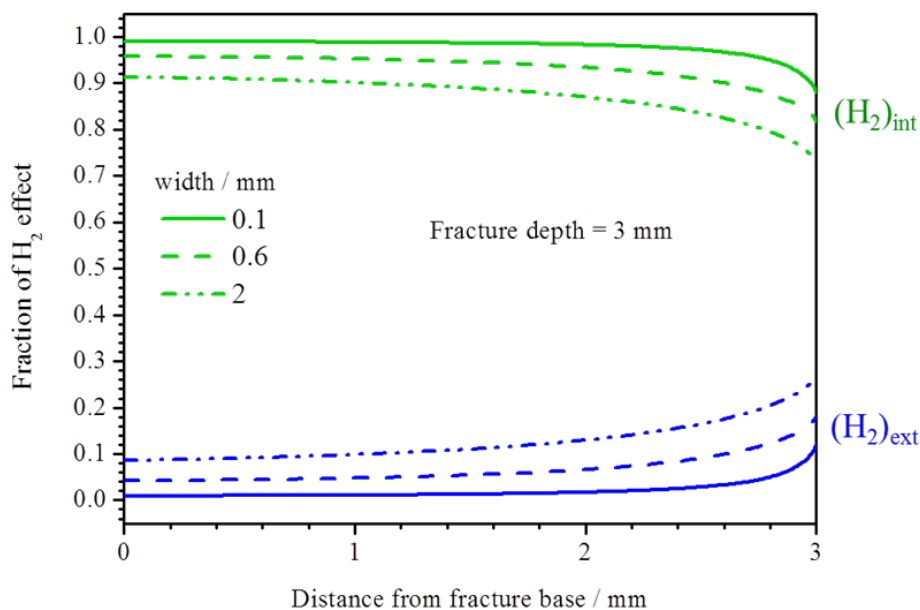

Figure 7. The fractional influences of $(H_2)_{int}$ (green) and $(H_2)_{ext}$ (blue) for different fracture widths (0.1, 0.6, and 2 mm) with a constant fracture depth (3 mm); $[H_2]_{bulk} = 10^{-8}$ M; all other model parameters have the default values.

6. Conclusion

A previously developed 2-D model for the corrosion of spent nuclear fuel inside a failed Cu-coated steel nuclear waste container emplaced in a geologic repository has been adapted to consider the influence of the redox-controlling reactions occurring within fractures in the fuel. The importance of the fractures is that they can act as locations at which H_2O_2, produced by the α-radiolysis of H_2O, can accumulate and be partially isolated from the redox scavengers (H_2, Fe^{2+}) produced by corrosion of the steel vessel, thereby leading to an increase in fuel corrosion rate.

By separating the influences on corrosion of radiolytic H_2 $((H_2)_{int})$ and H_2 from steel corrosion $((H_2)_{ext})$ the model shows their relative influence is strongly affected by the dimensions of fractures in the fuel and by the amount of H_2 produced by corrosion. If only small amounts of H_2 are produced by steel corrosion then radiolytic H_2 exerts the dominant influence on fuel corrosion since the transport of $(H_2)_{int}$ out of the fracture is limited especially if it is deep and narrow. Even when larger amounts of H_2 are

produced by steel corrosion, radiolytic H_2 remains the dominant reductant suppressing fuel corrosion in deep narrow fractures.

A number of mechanistic details and kinetic deficiencies remain unresolved. The kinetics of reactions involving H_2, H_2 and H_2O_2 and the decomposition of H_2O_2 (to O_2 and H_2O) are not known within the concentration ranges important for spent nuclear fuel. While these deficiencies may be covered by conservative assumptions in the calculations presented, they preclude any attempts to validate the model.

7. Reference

[1] Nuclear Waste Management Organization (NWMO), "Choosing a Way Forward: The Future Management of Canada's Used Nuclear Fuel", (Available at www.nwmo.ca), 2005.

[2] J. McMurry, D.A. Dixon, J.D. Garroni, B.M. Ikeda, S. Stroes-Gascoyne, P. Baumgartner, T.W. Melnyk, "Evolution of a Canadian Deep Geologic Repository: Base Scenario", Ontario Power Generation report: 06819-REP-01200-10092-R00, 2003.

[3] D.W. Shoesmith, F. King, B.M. Ikeda, "An Assessment of the Feasibility of Indefinite Containment of Canadian Nuclear Fuel Wastes", AECL-10972 COG-94-534, 1995.

[4] F. King and M. Kolar, "The Copper Container Corrosion Model Used in AECL's Second Case Study", Ontario Power Generation report: 06819-REP-01200-10041-R00, 2000.

[5] E. Ekeroth, O. Roth, M. Jonsson, "The Relative Impact of Radiolysis Products in Radiation Induced Oxidative Dissolution of UO_2", Journal of Nuclear Materials, Vol. 355, 2006, pp. 38-46.

[6] D.W. Shoesmith, "Fuel corrosion processes under waste disposal conditions", Journal of Nuclear Materials, Vol. 282, 2000, pp. 1-31.

[7] T.E. Eriksen, D.W. Shoesmith, M. Jonsson, "Radiation induced dissolution of UO_2 based nuclear fuel – A critical review of predictive modelling approaches", Journal of Nuclear Materials, Vol. 420, 2012, pp. 409-423.

[8] D.W. Shoesmith, M. Kolar, F. King, "A Mixed-Potential Model to Predict Fuel (Uranium Dioxide) Corrosion within a Failed Nuclear Waste Container", CORROSION, Vol. 59, 2003, pp. 802-815.

[9] M. Jonsson, F. Nielsen, O. Roth, E. Ekeroth, S. Nilsson, M.M. Hossain, "Radiation Induced Spent Nuclear Fuel Dissolution under Deep Repository Conditions", Environ. Sci. Technol, Vol. 41, 2007, pp. 7087-7093.

[10] D.W. Shoesmith, "Used Fuel and Uranium Dioxide Dissolution Studies – A Review", Report NWMO TR-2007-03, Nuclear Waste Management Organization, Toronto, ON, 2007.

[11] L. Wu, Z. Qin, D.W. Shoesmith, "An improved model for the corrosion of used nuclear fuel inside a failed waste container under permanent disposal conditions", Corrosion Science, Vol. 84, 2014, pp.85-95.

[12] L. Wu, Y. Beauregard, Z. Qin, S. Rohani, D.W. Shoesmith, "A model for the

influence of steel corrosion products on nuclear fuel corrosion under permanent disposal conditions", Corrosion Science, Vol. 61, 2012, pp. 83-91.

[13] F. Garisto, Barber, D.H., Chen, E., Inglot, A., and Morrison, C.A., "Alpha, Beta and Gamma Dose Rates in Water in Contact with Used CANDU Fuel", Report NWMO TR-2009-27, Nuclear Waste Management Organization, Toronto, ON, 2009.

[14] S. Nilsson, M. Jonsson, "On the catalytic effect of Pd(s) on the reduction of UO_2^{2+} with H_2 in aqueous solution", Journal of Nuclear Materials, Vol. 374, 2008, pp. 290-292.

[15] S. Nilsson, M. Jonsson, "On the catalytic effects of $UO_2(s)$ and Pd(s) on the reaction between H_2O_2 and H_2 in aqueous solution", Journal of Nuclear Materials, Vol. 372, 2008, pp. 160-163.

[16] S. Nilsson, M. Jonsson, "H_2O_2 and radiation induced dissolution of UO_2 and SIMFUEL pellets", Journal of Nuclear Materials, Vol. 410, 2011, pp. 89-93.

[17] R. Pehrman, M. Trummer, C.M. Lousada, M. Jonsson, "On the redox reactivity of doped UO2 pellets – Influence of dopants on the H_2O_2 decomposition mechanism", Journal of Nuclear Materials, Vol. 430, 2012, pp. 6-11.